ASTROBIOLOGY
Volume 7, Number 4, 2007

DOI: 10.1089/ast.2006.0098

Special Paper

Ultrastructural and Geochemical Characterization of Archean–Paleoproterozoic Graphite Particles: Implications for Recognizing Traces of Life in Highly Metamorphosed Rocks

JAMES D. SCHIFFBAUER,[1] LEIMING YIN,[2] ROBERT J. BODNAR,[1] ALAN J. KAUFMAN,[3] FANWEI MENG,[2] JIE HU,[2] BING SHEN,[1] XUNLAI YUAN,[4] HUIMING BAO,[5] and SHUHAI XIAO[1]

ABSTRACT

Abundant graphite particles occur in amphibolite-grade quartzite of the Archean–Paleoproterozoic Wutai Metamorphic Complex in the Wutaishan area of North China. Petrographic thin section observations suggest that the graphite particles occur within and between quartzite clasts and are heterogeneous in origin. Using HF maceration techniques, the Wutai graphite particles were extracted for further investigation. Laser Raman spectroscopic analysis of a population of extracted graphite discs indicated that they experienced a maximum metamorphic temperature of 513 ± 50°C, which is consistent with the metamorphic grade of the host rock and supports their indigenicity. Scanning and transmission electron microscopy revealed that the particles bear morphological features (such as hexagonal sheets of graphite crystals) related to metamorphism and crystal growth, but a small fraction of them (graphite discs) are characterized by a circular morphology, distinct marginal concentric folds, surficial wrinkles, and complex nanostructures. Ion microprobe analysis of individual graphite discs showed that their carbon isotope compositions range from −7.4‰ to −35.9‰ V-PDB (Vienna Pee Dee Belemnite), with an average of −20.3‰, which is comparable to bulk analysis of extracted carbonaceous material.

The range of their size, ultrastructures, and isotopic signatures suggests that the morphology and geochemistry of the Wutai graphite discs were overprinted by metamorphism and their ultimate carbon source probably had diverse origins that included abiotic processes. We considered both biotic and abiotic origins of the carbon source and graphite disc morphologies and cannot falsify the possibility that some circular graphite discs characterized by mar-

[1]Department of Geosciences, Virginia Polytechnic Institute and State University, Blacksburg, Virginia.
[2]Nanjing Institute of Geology and Paleontology, Nanjing, China.
[3]Department of Geology, University of Maryland, College Park, Maryland.
[4]State Key Laboratory of Palaeontology and Stratigraphy, Nanjing Institute of Geology and Palaeontology, Chinese Academy of Sciences, Nanjing, China.
[5]Department of Geology and Geophysics, Louisiana State University, Baton Rouge, Louisiana.

ginal folds and surficial wrinkles represent deflated, compressed, and subsequently graphitized organic-walled vesicles. Together with reports by other authors of acanthomorphic acritarchs from greenschist-amphibolite–grade metamorphic rocks, this study suggests that it is worthwhile to examine carbonaceous materials preserved in highly metamorphosed rocks for possible evidence of ancient life. Keywords: Archean—Paleoproterozoic—Acritarch—Wutai Metamorphic Complex—Jingangku Formation—Graphite discs—Amphibolite-grade metamorphism. Astrobiology 7, 684–704.

INTRODUCTION

When one assesses the early record of life, it quickly becomes apparent that two distinct and incongruent stories are evident: Proterozoic fossils are abundant and widely accepted, but Archean body fossils are few and controversial. Proterozoic acritarchs (a polyphyletic group of organic-walled vesicular microfossils) recovered from relatively unmetamorphosed cherts and shales provide a great deal of information about the evolution of early cellular life (Knoll *et al.*, 2006). Some Proterozoic acritarchs, such as those recovered from the ~1.5 Ga Ruyang and Roper Groups (Xiao *et al.*, 1997; Javaux *et al.*, 2001, 2003), have been interpreted to be among the earliest representatives of eukaryotic life in the fossil record. Paleontologists have also been able to identify evolutionary patterns, including both taxonomic diversity and morphological disparity patterns, from the fossil record of Proterozoic acritarchs (Knoll, 1994; Vidal and Moczydlowska-Vidal, 1997; Huntley *et al.*, 2006; Knoll *et al.*, 2006).

In contrast, the Archean fossil record is based upon a limited number of often controversial microfossils, biologically mediated sedimentary structures, and isotopic biosignatures. Filamentous structures from ~3.5 Ga low metamorphic grade cherts in Australia have been interpreted as bacterial fossils (Schopf and Packer, 1987; Schopf, 1993; Schopf *et al.*, 2002) or carbonaceous structures shaped by crystal growth (Brasier *et al.*, 2002, 2005, 2006), though less controversial microfossils have been known from Neoarchean rocks (Altermann and Schopf, 1995). Similarly, stromatolitic forms have been interpreted as structures produced by either physio-chemical (Lowe, 1994; Grotzinger and Rothman, 1996; Grotzinger and Knoll, 1999) or biological processes (Hofmann *et al.*, 1999; Allwood *et al.*, 2006). Even more controversial are isotopically light graphite particles from ~3.8 Ga amphibolite–metamorphic–grade banded iron-formations of West Greenland, which have been interpreted as products of early biological activity (Mojzsis *et al.*, 1996; Rosing, 1999; Mojzsis and Harrison, 2000) or metasomatic products of siderite decomposition under high temperature and pressure (Fedo and Whitehouse, 2002; van Zuilen *et al.*, 2002, 2003; Lepland *et al.*, 2005). Adding to the controversy is laboratory demonstration that abiotic pathways such as siderite decomposition and Fischer-Tropsch–type synthesis from CO_2–CH_4 fluids catalyzed by iron may lead to the formation of carbonaceous compounds depleted in ^{13}C (van Zuilen *et al.*, 2002; Horita, 2005; McCollom and Seewald, 2006). Thus, the above-mentioned complications necessitate a great deal of caution to be implemented and demand multiple lines of evidence (morphological, ultrastructural, and geochemical) to be sought during the interpretation of Archean and early Paleoproterozoic biosignatures.

In addition to the controversies surrounding the geobiological evidence of early life, the study of Archean life is also limited by the predominance of high-metamorphic–grade rocks. It is traditionally accepted that high-grade metamorphism is detrimental to morphological fossil preservation. Accordingly, Archean microfossils with recognizable biological morphologies previously have been reported only from low-grade metacherts (Knoll and Barghoorn, 1977; Awramik *et al.*, 1983; Schopf and Walter, 1983; Walsh and Lowe, 1985; Altermann and Schopf, 1995). However, recent studies of Precambrian and Phanerozoic rocks have shown that *bona fide* filamentous bacteria, organic-walled microfossils (*e.g.*, leiospheres, acanthomorphic acritarchs, and chitinozoans), and possible paraconodonts can be preserved in greenschist-grade metamorphic rocks (Kidder and Awramik, 1990; Knoll, 1992; Molyneux, 1998), greenschist-amphibolite–grade rocks (Squire *et al.*, 2006; Zang, 2007), and gneisses (Hanel *et al.*, 1999).

These recent developments prompted us to explore highly metamorphosed rocks of the

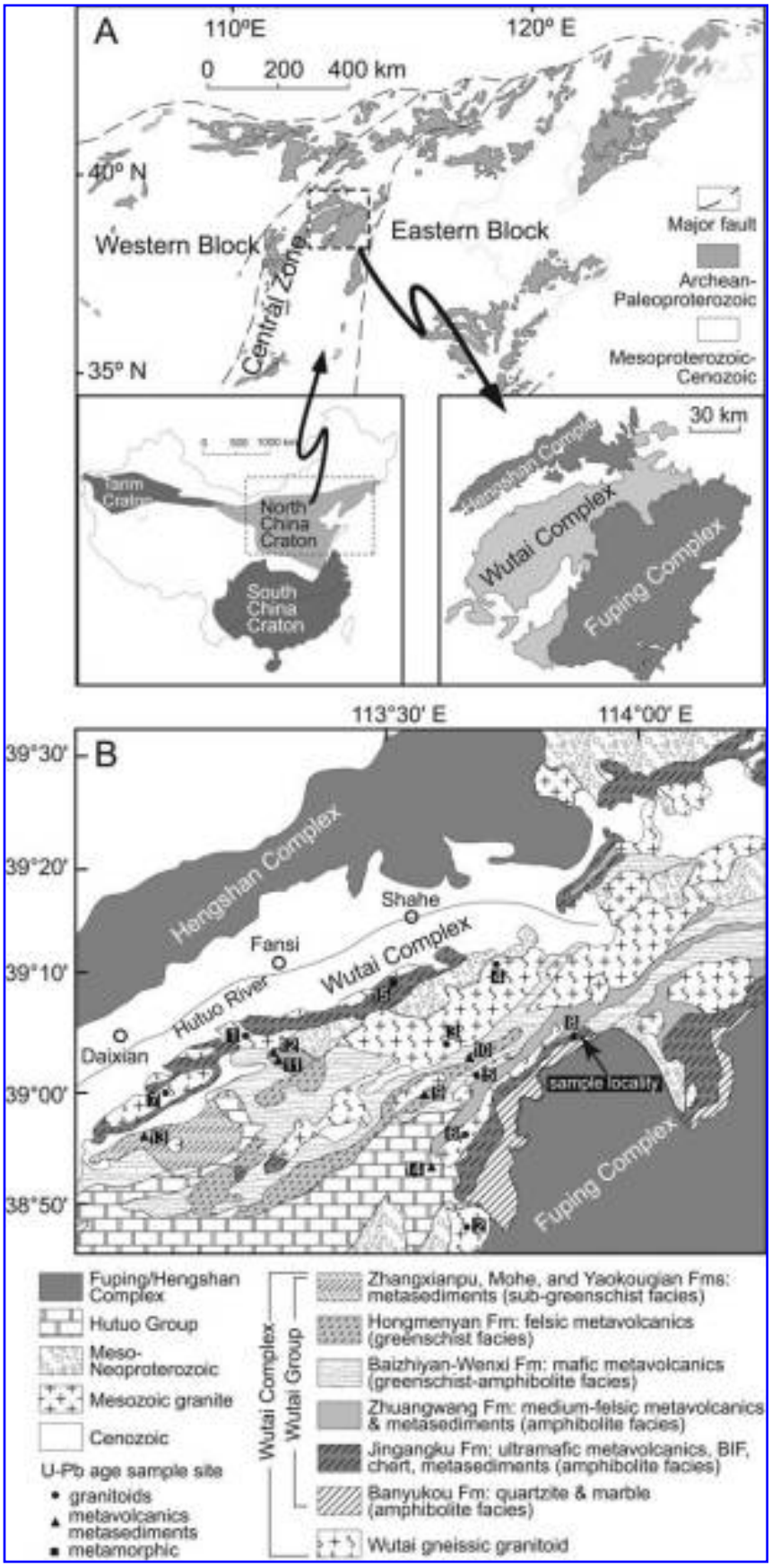

FIG. 1. Geological map and sample locality. (**A**) Location of Wutai Metamorphic Complex in the Central Zone. Insets show the North China Craton (lower left) and the Wutai Complex sandwiched between the Fuping and Hengshan complexes (lower right). (**B**) Geological map of the Wutai Complex. The eight formations of the Wutai Group are coded and listed in stratigraphic order according to Tian (1991). Numbered dots denote sampling sites of U–Pb radiometric dates (Table 1).

Archean–early Paleoproterozoic Wutai Metamorphic Complex in the Wutaishan area of North China, using a combination of light microscopy, electron microscopy, Raman spectroscopy, and ion microprobe techniques. The immediate goal of this study was to characterize the morphological, ultrastructural, and geochemical features of the carbonaceous material recovered from the Wutai Metamorphic Complex. Our study resulted in the recovery of abundant graphite particles from amphibolite-grade quartzites of the Wutai Metamorphic Complex in the Wutaishan area of North China. Raman spectroscopy indicated that these graphite particles are indigenous to the host rock. Most graphite particles are irregular in shape and show hexagonal broken edges, but a distinct population of graphite particles can be characterized as circular discs with marginal folds and surficial wrinkles. Although the morphology of these graphite discs must have been overprinted by fragmentation, crystal growth, and other abiotic processes, the presence of marginal folds and surficial wrinkles on circular discs seems to suggest that they may represent deflated, compressed, and subsequently graphitized organic-walled vesicles. Transmission electron microscopy shows that they appear to consist of two graphitized layers separated by an electron-dense material trapped in between. Isotopic analysis of bulk carbonaceous material gave a carbon isotope value of −21.3‰ V-PDB, but ion probe analysis of individual graphite particles gave a range of carbon isotope values between −7.4‰ and −35.9‰ V-PDB, with an average of −20.3‰. At the present, the morphological, ultrastructural, and geochemical evidence for a biological origin is still equivocal, but this study represents a first attempt to characterize carbonaceous material from highly metamorphosed Archean–early Paleoproterozoic rocks using a combination of analytical tools.

GEOLOGICAL SETTING

The Wutai Metamorphic Complex is located between the Fuping and Hengshan metamorphic complexes, which together compose the middle segment of the Trans-North China Orogen and constitute the Hengshan-Wutai-Fuping mountain belt. The Trans-North China Orogen is a narrow northeast-southwest zone, also known as the Central Zone, which separates the eastern and western blocks of the North China Craton (Fig. 1A). Three different tectonic models have been proposed for the development and evolution of the Hengshan-Wutai-Fuping mountain belt. The first suggests that the Fuping and Hengshan complexes were part of a single continental block, and the Wutai complex was formed in a late Archean rift basin between the Fuping and Hengshan complexes (Tian, 1991; Yuan and Zhang, 1993). The second model suggests that the Hengshan-Wutai-Fuping mountain belt represents a late Archean continent-arc-continent collision system, with the Hengshan and Fuping complexes corresponding to two Archean continental blocks, and the Wutai complex representing the trapped intermediate island arc (Bai, 1986; Li *et al.*, 1990; Bai *et al.*, 1992; Wang *et al.*, 1996). As a third model, recent data suggest that these complexes represent a single late Archean to early Paleoproterozoic magmatic arc that underwent deformation, metamorphism, and exhumation, and was subsequently incorporated into the Trans-North China Orogen in the development of the North China Craton (Zhao *et al.*, 2004).

The Wutai Metamorphic Complex is a greenstone terrane that consists of tonalitic-trondhjemitic-granodioritic gneisses, granitoids, mafic to felsic volcanic rocks, and metamorphosed volcanic-sedimentary rocks (Polat *et al.*, 2005). On the basis of metamorphic facies and geological mapping, the volcanic-sedimentary package of the Wutai Metamorphic Complex has been classified as the Wutai Group (Fig. 1B), which is subdivided into eight formations (Tian, 1991). The lower Wutai Group consists mainly of amphibolite, orthogneiss, and metasedimentary rocks, including banded iron-formation and quartzite metamorphosed to lower amphibolite facies. Petrographic study indicates that the lower Wutai Group was heated to a maximum temperature of 600–650°C and buried to a maximum pressure of 10–12 kbar (Zhao *et al.*, 1999). The middle Wutai Group is composed of greenschist facies tholeiites and felsic volcanics. The upper Wutai Group consists of greenschist to subgreenschist facies metasediments and metavolcanics. The Wutai Metamorphic Complex is unconformably overlain by the Hutuo Group, which is comprised of subgreenschist facies metasediments and minor mafic volcanics, including quartzites, slates, and metabasalts.

Recent geochronological data from SHRIMP (Sensitive High Resolution Ion Microprobe) U–Pb

zircon analyses of samples from the lower, middle, and upper subgroups of the Wutai Group (Wilde *et al.*, 2004a), however, suggest that these units are roughly of similar age. For example, Wilde *et al.* (2004a) reported eight SHRIMP zircon U–Pb ages from intermediate to felsic volcanic rocks of the lower, middle, and upper subgroups. These eight ages range from 2533 ± 8 to 2513 ± 8 Ma, and together they give a weighted mean of 2523 ± 3 Ma. These ages do not support correlation between age and metamorphic grade of the three subgroups as had been previously suggested (Bai, 1986; Tian, 1991). Therefore, metamorphic grade cannot be used as a stratigraphic indicator within the Wutai Group (Wilde *et al.*, 2004a), and the geochronological data cast doubt on the superposition relationship of the units within the Wutai Group (Bai, 1986; Tian, 1991).

Regardless of the controversy that surrounds the stratigraphic relationship of the Wutai Group, there is ample geochronological data to suggest that the Wutai Complex and Hutuo Group are Archean–early Paleoproterozoic in age (Table 1). The Wutai Group is penetrated by gneissic granitoids and granitoids that were emplaced pre-, syn-, and post-greenstone metamorphism (Tian, 1991; Wilde *et al.*, 2005). Extensive radiometric dating shows three episodes of granite intrusion, during 2560–2540 Ma, 2540–2515 Ma, and 2170–2120 Ma; the 2540–2515 Ma granitoids were interpreted as coeval with felsic volcanism in the Wutai Complex (Wilde *et al.*, 2005). Metavolcanics in the Wutai Group range from 2533 ± 8 Ma to 2513 ± 8 Ma (Wilde *et al.*, 2004a), which further confirms an Archean age for the Wutai Group. A volcanic ash from the overlying Hutuo Group gave a SHRIMP U–Pb zircon age of 2087 ± 9 Ma (Wilde *et al.*, 2004b). Therefore, the age of the Wutai Metamorphic Complex is conservatively constrained from late Archean to early Paleoproterozoic.

Our samples were collected from a 10–30 cm thick bed of carbonaceous quartzite (Fig. 2C) in a geological unit mapped as the Jingangku Formation of the Wutai Group, near the village of Shentangpu (39°07.386′N, 113°55.223′E; Fig. 2A). The Jingangku Formation consists of ultramafic volcanics, amphibolite, iron-formation (Fig. 2B), volcanogenic massive sulfide deposit, and metasedimentary rocks, including micaschist, calc-silicate, and quartzite (Tian, 1991; Polat *et al.*, 2005). The metavolcanics are interpreted as "remnants of oceanic crust," whereas the metasedimentary rocks as "stable continental margin sediments" (Polat *et al.*, 2005).

Some geologists (Wang *et al.*, 2000) argue that the geological unit mapped as the Jingangku Formation may entirely or partly belong to the Hutuo Group. Because the Wutai Complex can interfinger with the younger, less severely metamorphosed Hutuo Group in the Wutaishan area (Wilde *et al.*, 2004b), extreme care has been taken to ensure that our collected samples belong to the Jingangku Formation of the Wutai Complex. Our sampling locality is *ca.* 25 km northeast of the Wutai-Hutuo interfingering zone (Wilde *et al.*, 2004b). In addition, our sample locale was in close association with amphibolite and banded iron-formation (Fig. 2B), which are characteristic lithologies of the Jingangku Formation of the Wutai Complex but not characteristic of the Hutuo Group. Furthermore, Raman geothermometery of isolated graphite and petrographic analysis of our samples show that they are more akin to the amphibolite-grade metamorphism of the Wutai Complex, but inconsistent with the greenschist-grade metamorphism of the Hutuo Group in eastern Wutaishan area (Tian, 1991), where our samples were collected. More importantly, samples from the Jingangku Formation near our sampling locality yielded a 2508 ± 2 Ma U–Pb age that is interpreted to date the peak metamorphism of the Jingangku Formation (Table 1) (Liu *et al.*, 1985). Pyrite from the Jingangku Formation also yields ^{33}S anomalies (Ding *et al.*, 2004), which are consistent with its Archean age because ^{33}S anomalies are not known in geological samples younger than ~2.4 Ga (Bekker *et al.*, 2004). Therefore, our samples likely belong to the Jingangku Formation of the Wutai Complex, rather than to any stratigraphic units of the overlying Hutuo Group. Regardless, the conservative age estimate (Archean–Paleoproterozoic) of our samples stands even if they belong to the Hutuo Group (2087 ± 9 Ma; Wilde *et al.*, 2004b).

METHODS

Standard petrographic thin sections were made from the Jingangku carbonaceous quartzite samples and examined under a microscope using both plain and polarized light. In thin sections, quartzite clasts are set in a fine-grained carbonaceous (primarily graphitic) matrix. Graphite particles occur in both the matrix and clasts (Fig. 3A–H), which confirms their indigenicity.

TABLE 1. PUBLISHED U–PB ZIRCON AGES (CONVENTIONAL OR SHRIMP) OF THE WUTAI METAMORPHIC COMPLEX AND THE HUTUO GROUP

Lithology	*Geological unit*	*Locality in Fig. 1B*	*U–Pb age (Ma) ± 2σ*	*Interpretation*	*Reference*	*Sample #*
Archean Granitoids in the Wutai Complex						
Granitoid	Ekou granite	1	2566 ± 13	Crystallization age	(Wilde *et al.*, 1997)	95PC34
Granitoid	Ekou granite	1	2555 ± 6	Crystallization age	(Wilde *et al.*, 1997)	95-19
Granitoid	Lanzhishan granite	2	2553 ± 8	Crystallization age	(Wilde *et al.*, 1997)	95PC94
Granitoid	Lanzhishan granite	2	2537 ± 10	Crystallization age	(Wilde *et al.*, 1997)	95PC96
Granitoid	Lanzhishan granite	2	2560 ± 6	Crystallization age	(Liu *et al.*, 1985)	Ag5-2,5
Granitoid	Chechang-Beitai granite	3	2538 ± 6	Crystallization age	(Wilde *et al.*, 2005)	WC-5
Granitoid	Chechang-Beitai granite	3	2546 ± 6	Crystallization age	(Wilde *et al.*, 2005)	WC-6
Granitoid	Chechang-Beitai granite	4	2552 ± 11	Crystallization age	(Wilde *et al.*, 2005)	WC-7
Granitoid	Chechang-Beitai granite	3	2551 ± 5	Crystallization age	(Wilde *et al.*, 2005)	95PC6B
Granitoid	Guangmingsi granite	5	2531 ± 5	Crystallization age	(Wilde *et al.*, 2005)	95PC76
Granitoid	Shifo granite	6	2531 ± 4	Crystallization age	(Wilde *et al.*, 2005)	95PC98
Granitoid	Wangjiahui granite	7	2520 ± 9	Crystallization age	(Wilde *et al.*, 2005)	95PC62
Granitoid	Wangjiahui granite	7	2517 ± 12	Crystallization age	(Wilde *et al.*, 2005)	95PC63
Metasedimentary or metavolcanic rocks of the Wutai Complex/Hutuo Group						
Garnet quartzite	Jingangku Formation*	Hengshan	2527 ± 10	Protolith age	(Wang *et al.*, 2000)	HG-5
Quartzite	Jingangku Formation*	Hengshan	2501 ± 15	Protolith age	(Wang *et al.*, 2000)	HG-7
Metavolcanics	Jingangku Formation	8	2438 ± 36	Protolith age	(Bai *et al.*, 1992)	not reported
Quartz keratophyre	Hongmenyan Formation	9	2522 ± 17	Protolith age	(Liu *et al.*, 1985)	Ag6-2
Metadacite	Hongmenyan Formation	10	2524 ± 8	Protolith age	(Wilde *et al.*, 2004a)	WT-17
Metavolcanics	Hongmenyan Formation	10	2516 ± 10	Protolith age	(Wilde *et al.*, 2004a)	WT-12
Metavolcanics	Hongmenyan Formation	10	2533 ± 8	Protolith age	(Wilde *et al.*, 2004a)	WT-13
Metavolcanics	Hongmenyan Formation	10	2523 ± 9	Protolith age	(Wilde *et al.*, 2004a)	WT-9
Metavolcanics	Zhuangwang Formation	11	2529 ± 10	Protolith age	(Wilde *et al.*, 2004a)	96PC114
Metavolcanics	Zhuangwang Formation	12	2513 ± 8	Protolith age	(Wilde *et al.*, 2004a)	95PC3119
Metavolcanics	Baizhiyan Formation	12	2524 ± 10	Protolith age	(Wilde *et al.*, 2004a)	95PC3115
Metavolcanics	Upper Wutai Group	13	2528 ± 6	Protolith age	(Wilde *et al.*, 2004a)	95PC355C
Felsic tuff	Upper Wutai Group	13	2523 ± 18	Protolith age	(Kröner *et al.*, 2005)	95PC30
Metabolcanics	Hutuo Group	14	2087 ± 9	Volcanic ash age	(Wilde *et al.*, 2004b)	HTG-10
Metamorphic age						
Metavolcanics	Jingangku Formation	15	2508 ± 2	Metamorphic age	(Liu *et al.*, 1985)	Ag7-7

Sample localities are numbered and marked in Fig. 1B.
*These two sample horizons were considered by the authors (Wang *et al.*, 2000) as equivalents to the Northern Jingangku Formation in the Hengshan Complex.

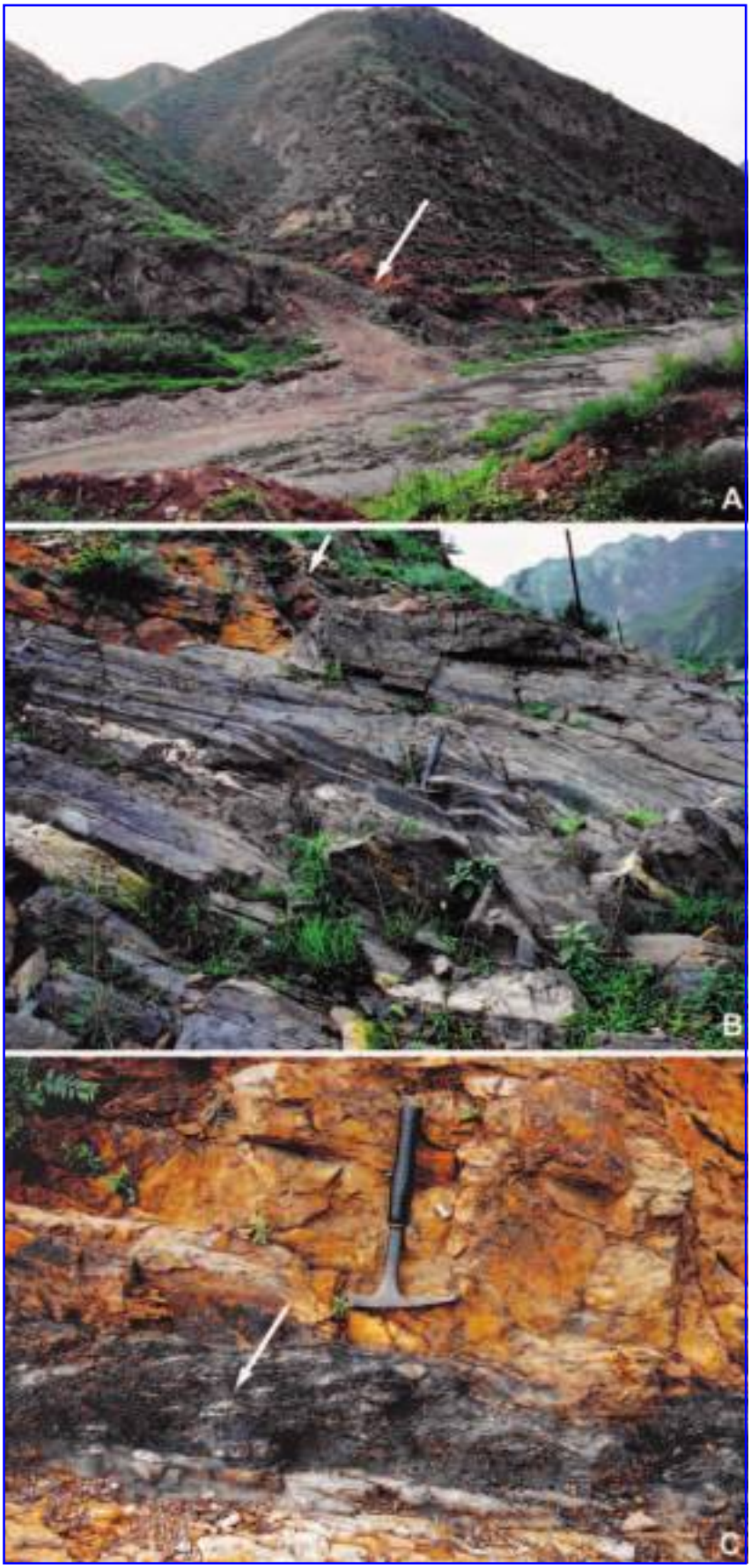

FIG. 2. Field photographs of sample horizon. (**A**) Field photograph of sample locality (arrow) near Shentangpu (39°07.386′N, 113°55.223′E). (**B**) Amphibolite (rock hammer) below and weathered iron-formation (arrow) above sample horizon. (**C**) Close-up of sampled unit of carbonaceous quartzite (arrow).

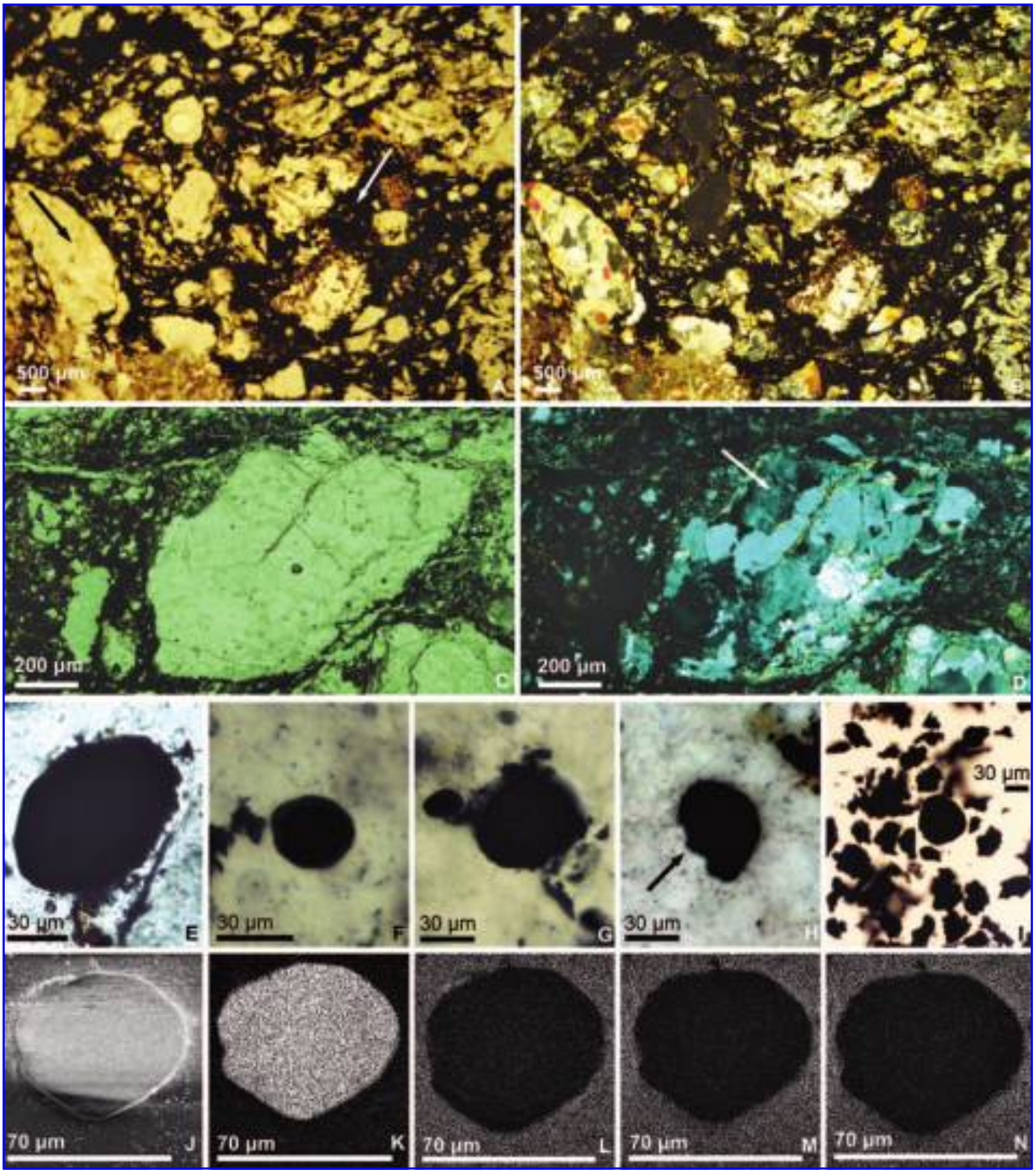

FIG. 3. Light microscopy and elemental mapping of *in situ* (A–G) and extracted (I–N) graphite particles. (**A**) Angular mm–cm sized clasts (black arrow) set in finer-grained carbonaceous matrix (white arrow). (**B**) Same as **A** viewed under cross nicols. Note multiple sand- to silt-sized quartz grains in clasts. (**C**) Close-up of a clast surrounded by matrix graphite. (**D**) Same as **C** viewed under cross nicols to show quartz grains within clast and undulose extinction (white arrow). (**E–H**) Photomicrographs of clast-hosted circular to elliptical graphite discs in thin sections. Specimen in **H** lies slightly oblique to the cut of the thin section, where part of the disc was polished away (black arrow). (**I**) Extracted carbonaceous material, the bulk of which has irregular morphology. Note, at center of image, a circular disc with a diameter of ~60 μm. (**J**) SEM of uncoated specimen used for elemental maps. Carbon (**K**), calcium (**L**), oxygen (**M**), and silicon (**N**) elemental maps of specimen illustrated in **J**.

To extract graphite particles (20–220 μm, s.d. = 31 μm, n = 270; Fig. 4), ~30–50 g rock chips were immersed in concentrated hydrochloric acid and then 48–51% hydrofluoric acid for a week. Carbonaceous residue (Fig. 3I), including abundant graphite particles, was recovered from acid maceration. The carbonaceous nature of extracted graphite particles was confirmed by elemental mapping (Fig. 3J–N) and electron microprobe analysis (Fig. 5). To verify the indigenicity of the graphite particles, we used Raman spectroscopy to estimate their peak metamorphic temperature, following the method described in Beyssac *et al.* (2002). Raman microprobe analyses were carried out on both *in situ* graphite particles (eight specimens within matrix, Fig. 6A–B; eight specimens within clasts, Fig. 7A–B) and extracted, subcircular to circular graphite discs (twelve specimens, Fig. 8A–B). Raman microprobe analysis was performed on a Dilor X-Y Raman microprobe system (Virginia Tech, 514.32 nm laser focused to a diameter of <20 μm under a 40× objective, laser power 100 mW) and a JY LabRam HR800 Raman microprobe system (Virginia Tech, 632.81 nm laser focused to a diameter of <20 μm under a 40× objective, laser power 25 mW). To test whether the orientation of *in situ* graphite particles had any effect on Raman microprobe analysis, Raman spectra of the same particles were collected with the thin section rotated at 0°, 90°, 180°, and 270° (Fig. 9). Background noise of Raman spectra in Figs. 6A–B and 7A–B was reduced using the Savitzky-Golay smoothing method (6th order polynomial with 40 points per sample) conducted on GRAMS/AI software.

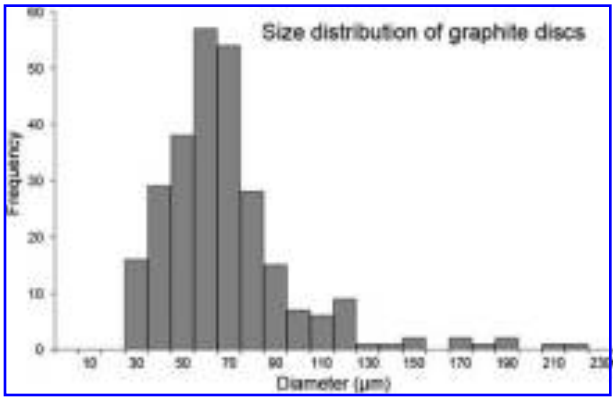

FIG. 4. Size distribution of graphite discs (mean = 64 μm, s.d. = 31 μm, n = 270).

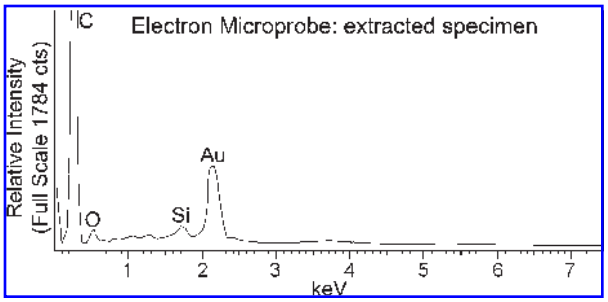

FIG. 5. Electron microprobe analysis of a Jingangku specimen. X-ray energy dispersive spectrum shows a sharp carbon spike. Gold peak due to gold coating.

Extracted graphite particles were examined under a light microscope, and circular to sub-circular graphite discs were manually removed from carbonaceous residue for electron microscopy analyses (Fig. 10). Scanning electron microscopy (SEM), field emission scanning electron microscopy (FE-SEM), and transmission electron microscopy (TEM) were performed on LEO 1550 FE-SEM (Virginia Tech), JEOL JSM 6300 (Nanjing), LEO 1530 VP (Nanjing), and Zeiss DSM 982 (Maryland) electron microscopes. FE-SEM observations of magnifications up to 200,000× achieved 5 nm resolution. Electron microprobe and elemental mapping analyses were performed on an INCA energy dispersive X-ray spectroscopy system attached to an LEO 1530 VP electron microscope (Nanjing). Several specimens were imbedded in epoxy, and then ultra thin (~60 nm) sections were microtomed for TEM observations (JEOL JEM-1230 in Nanjing).

Carbon isotopes of bulk carbonaceous material (*i.e.*, acid macerates) were analyzed using a conventional combustion method in Nanjing (Finnigan MAT 251 mass spectrometer) and at the University of Maryland (Micromass IsoPrime dual-inlet gas source stable isotope mass spectrometer, coupled with a Eurovector elemental analyzer). Analytical precision was better than 0.1‰ versus V-PDB. Eleven $\delta^{13}C$ measurements (Table 2) were conducted on five specimens using a Cameca 6f ion microprobe (Carnegie Institution of Washington). The magnitude of instrumental mass fractionation (IMF) inherent to surface ionization mass spectrometry was quantified by the repeated analyses of the standard Mao diamond ($\delta^{13}C = -6.5‰$, IMF = 52.9 ± 0.5‰, n = 9, Table 2). The primary Cs^+ beam intensity was 0.5 nA and was focused down to a

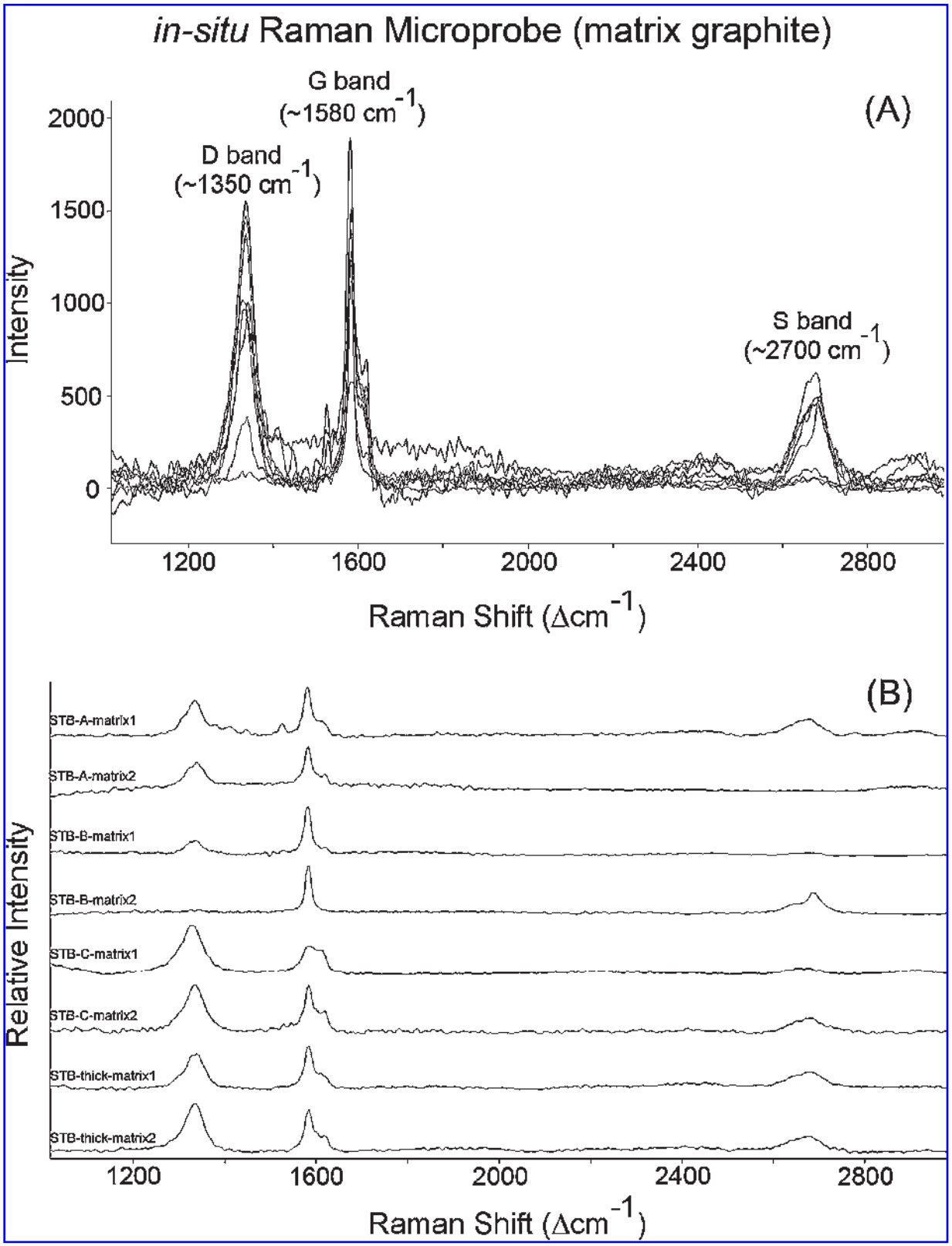

FIG. 6. ***In situ*** **laser Raman analyses of 8 matrix graphite particles.** Note variation in D band. All spectra have been baseline corrected and smoothed using the Savitzky-Golay method. (**A**) All spectra superimposed on each other. (**B**) Individual spectra.

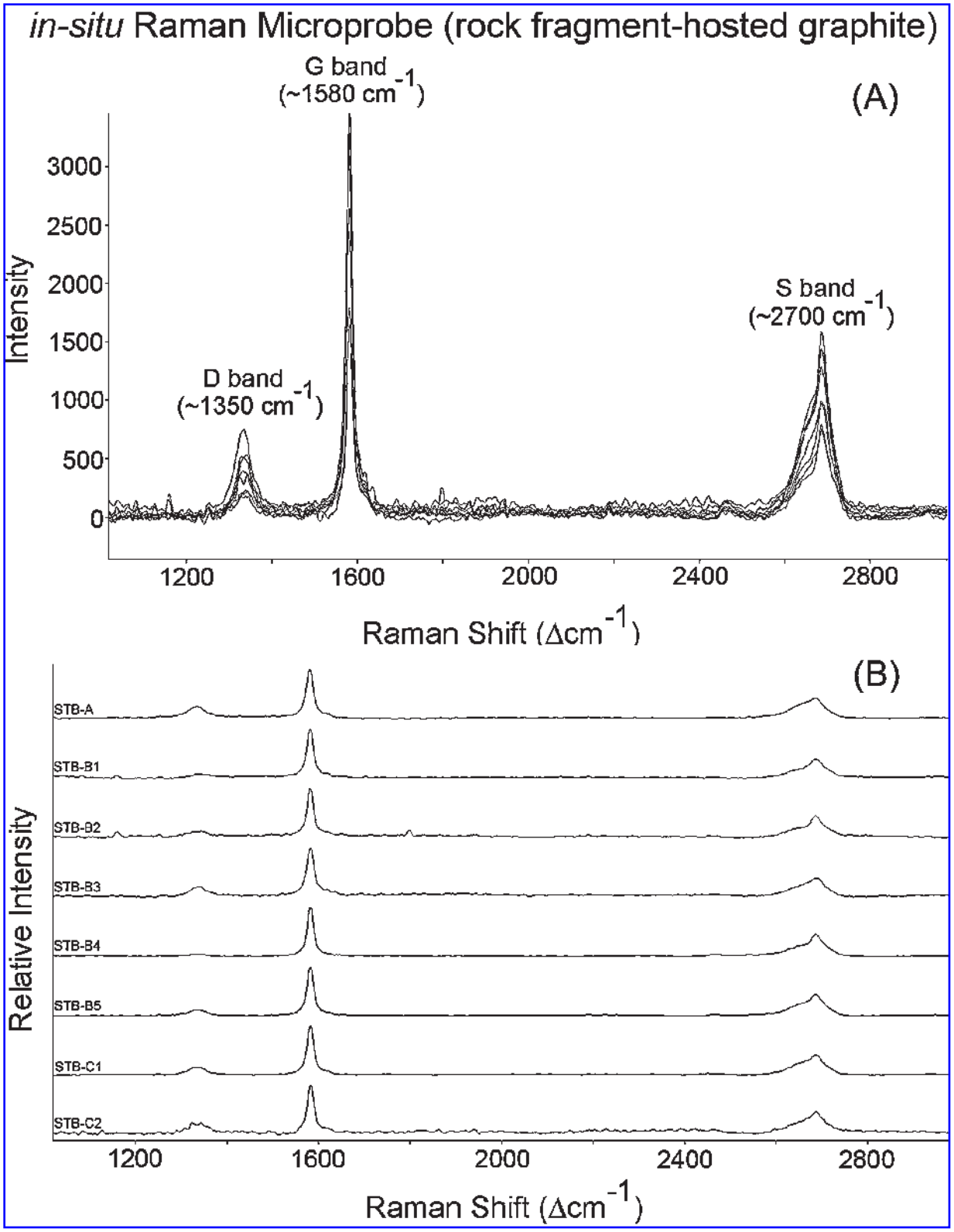

FIG. 7. ***In situ*** **laser Raman analyses of 8 clast-hosted graphite particles.** Note consistently low intensity of D band. All spectra have been baseline corrected and smoothed using the Savitzky-Golay method. (**A**) All spectra superimposed on each other. (**B**) Individual spectra.

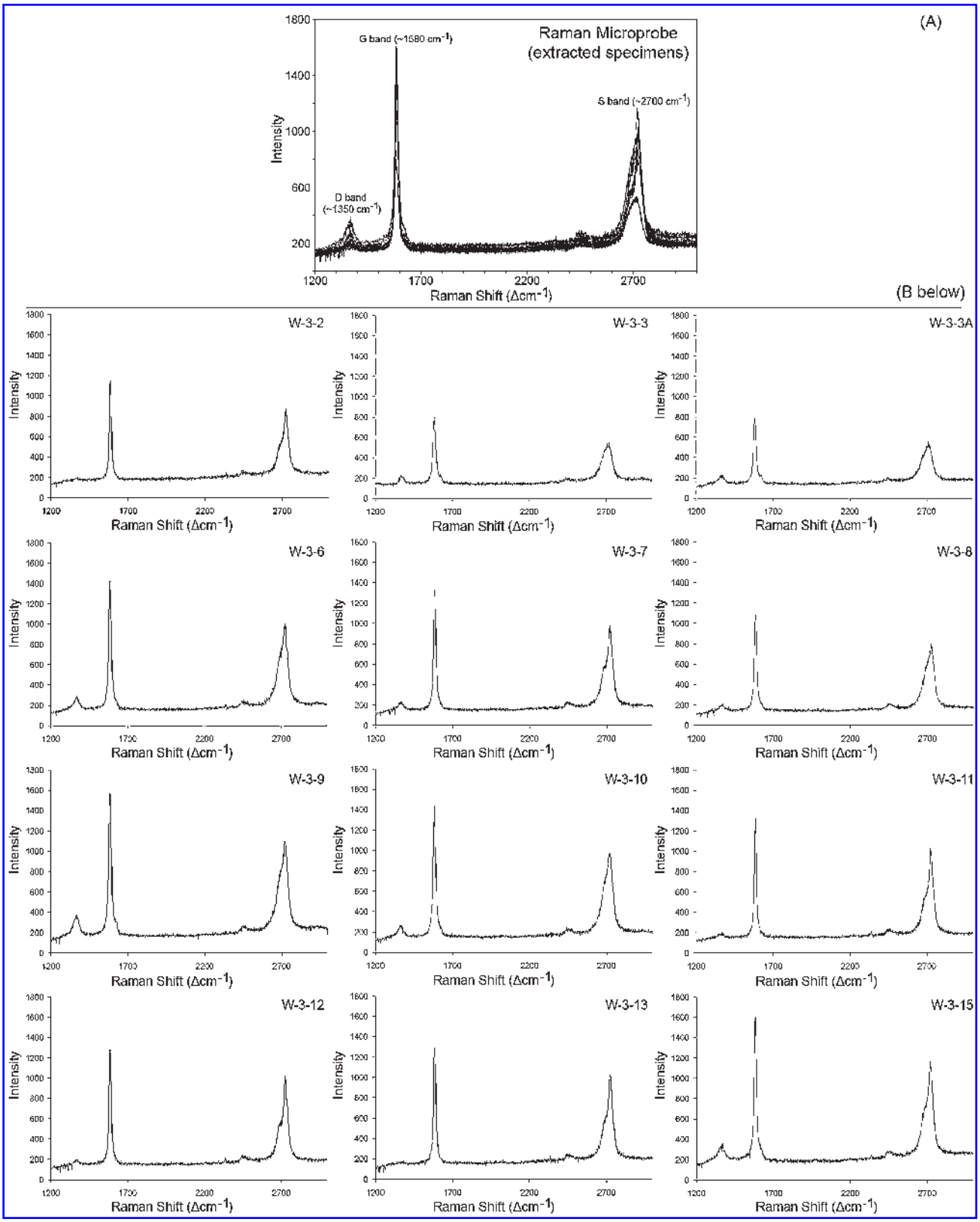

FIG. 8. Laser Raman spectra of 12 extracted graphite discs. Note consistently low intensity of D band and similarity to Raman spectra of clast-hosted graphite particles. Spectra are not baseline corrected. (**A**) All spectra superimposed on each other. (**B**) Individual spectra.

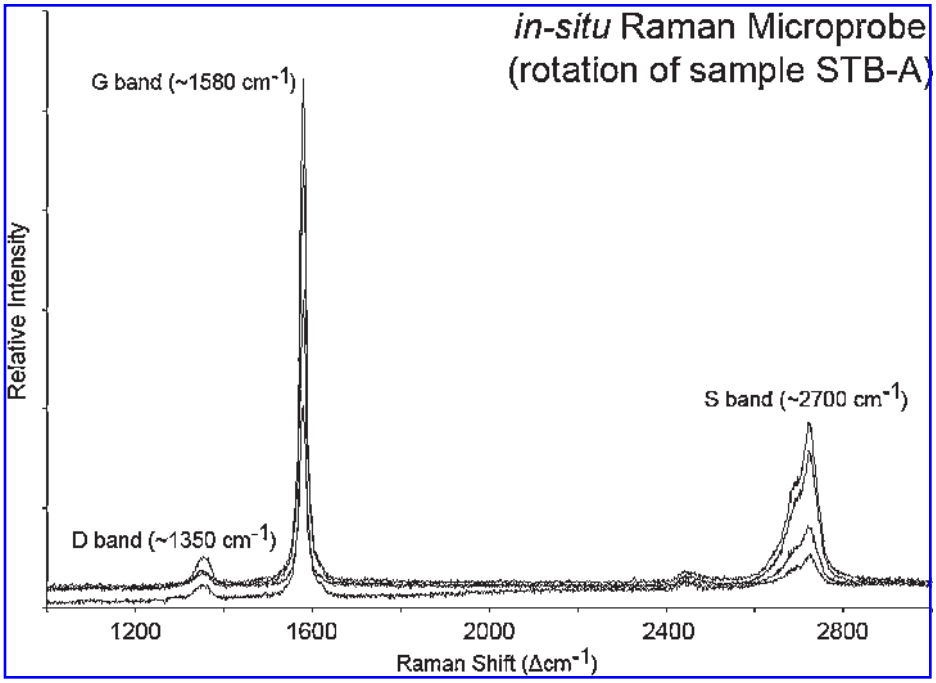

FIG. 9. ***In situ*** **rotational analysis of a Jingangku graphite particle in thin section.** Spectra were collected at 4 orientations: 0°, 90°, 180°, and 270°. The relative intensity of the D and G bands does not change significantly with rotation angles, although the S band shows slight variation. Spectra are not baseline corrected.

20–25 μm spot, which allowed for multiple analyses of the same individual specimen.

RESULTS

Petrographic analysis of the sampled Jingangku carbonaceous quartzite showed strong brecciation, with angular mm- to cm-sized rock fragments set in finer-grained, carbonaceous matrix (Fig. 3A–B). The rock fragments (or clasts) were not elongated or preferentially oriented and consisted of randomly oriented sand- to silt-size quartz minerals (Fig. 3A–D), as well as minor carbonate minerals. Most quartz grains showed undulose extinction (Fig. 3D), which indicates modification of optical axes by metamorphic stress. The composite clasts require at least two genera-

FIG. 10. SEM and TEM images of Jingangku graphite discs. (**A**) Vial containing graphitized discs and carbonaceous matter extracted from 30 g rocks. Scale in cm. (**B**) Representative filament extracted along with graphitized discs. (**C**) Circular to elliptical disc with concentric marginal folds and amorphous carbonaceous material on surface. (**D**) Magnified view of arrowed area in **C** showing concentric marginal folds. Arrow points to plunging and tapering fold. **(E)** Circular to elliptical disc similar to **C** with concentric marginal folds. (**F**) Elliptical disc with crescentic folds in upper part and featureless graphite sheets in lower part. (**G**) Detail of crescentic folds in upper right margin of **F**. (**H**) Subhedral specimen with irregular surficial wrinkles and fragmented edge (short arrows). (**I**) Details of surficial wrinkles in lower right of **H**. (**J**) Lower right edge (rotated) of **H**, illustrating marginal folds. (**K**) Folded, wrinkled, and fragmented (short arrows) disc. (**L**) Elliptical to subhedral specimen with fracture (long arrow). (**M**) Marginal folds on lower right margin of **L** (marked by short arrow). (**N**) Cross-sectional view along fracture in specimen **L** (marked by long arrow). Note central gap between two sets of graphite sheets. (**O**) Specimen with sharp bending (long arrow) and kinking (short arrow). (**P**) Flat sub-rounded to subhedral disc with marginal steps (arrow) representing termination of graphite sheets. (**Q**) Sub-rounded to subhedral disc with crescentic folds along upper half and graphite edge overgrowth in lower half. (**R**) High magnification SEM showing nanoridges on disc surface. (**S**) TEM of graphite disc showing poorly defined central gap (arrows). (**T**) TEM of graphite disc showing electron-dense layer (arrow). (**U**) High magnification SEM showing nanopores filled with material of high atomic mass. (**V**) Similar nanopores in vesicle walls of Mesoproterozoic acritarch *Dictyosphaera delicata*. Nanopores filled with aluminum phosphate minerals. **B–R** are SEM photomicrographs collected using secondary electron detector, **U–V** are SEM photomicrographs using back-scattered electron detector, and **S–T** are TEM photomicrographs. Scale bars represent 10 μm unless otherwise noted.

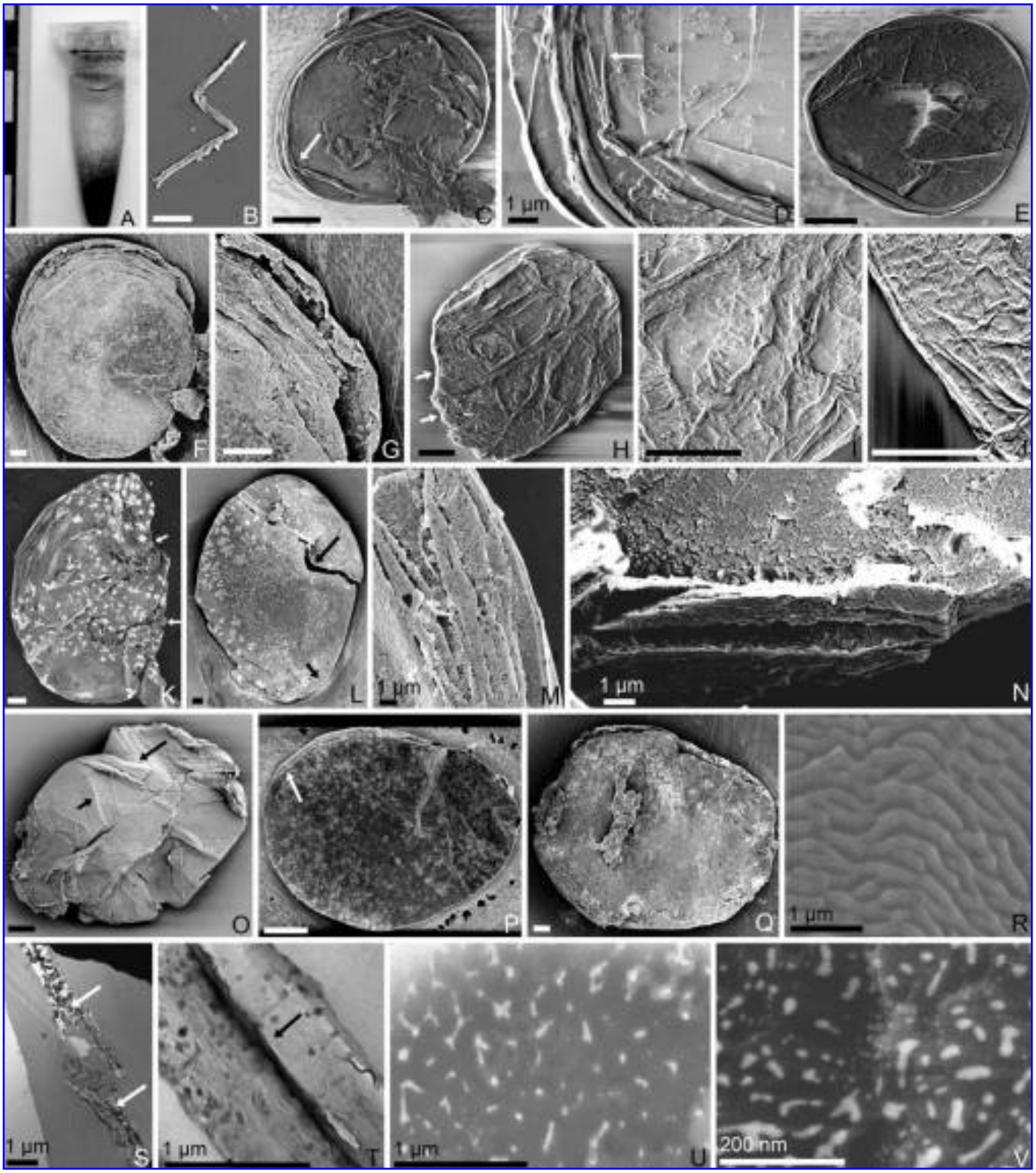

FIG. 10A–V.

TABLE 2. $\delta^{13}C$ MEASUREMENTS OF GRAPHITE DISC SPECIMENS AND MAO STANDARD (6.5% VERSUS V-PDB)

Analysis #	*Sample #*	$\delta^{13}C$	*Corrected* $\delta^{13}C$
1. Mao Standard		−59.83	
2. Mao Standard		−59.88	
3. Mao Standard		−59.40	
4. Sample	A3	−72.22	−19.3
5. Sample	A3	−70.50	−17.6
7. Sample	A2	−67.93	−15.0
8. Sample	A2	−62.91	−10.0
9. Sample	A2	−60.33	−7.4
10. Mao Standard		−59.98	
11. Mao Standard		−59.29	
13. Mao Standard		−58.97	
14. Mao Standard		−59.63	
15. Sample	B2	−88.84	−35.9
16. Sample	B2	−79.68	−26.8
17. Mao Standard		−59.49	
18. Sample	C2	−78.48	−25.6
19. Sample	C2	−80.07	−27.1
20. Sample	C4	−73.48	−20.6
21. Sample	C4	−71.47	−18.5
22. Mao Standard		−58.43	

tions of fragmentation; the more recent fragmentation was probably tectonic brecciation because of the strong angularity, whereas the earlier fragmentation appears to be sedimentary because of the moderate level of sorting. Heavy mineral analysis is being conducted to test this interpretation.

Our samples are moderately carbonaceous (two measurements of 0.72% and 1.06% total organic carbon (TOC), weight percentage determined by combustion analyses of one randomly crushed sample, sample weights used for analysis ~30 and ~50 g). The carbonaceous material consisted mostly of graphite particles. Their indigenicity and graphite nature were verified by thin section petrographic observations (Fig. 3A–H), elemental mapping (Fig. 3J–N), electron and Raman microprobe analyses (Figs. 5–9), and scanning electron microscopy (Fig. 10C–R, 10U–V). Graphite particles occur abundantly in the matrix between clasts (Fig. 3A–D), but less abundantly within clasts (Fig. 3E–H). Some clast-hosted graphite particles are circular to elliptical (Fig. 3E–H), but the morphology of matrix graphite is difficult to resolve under petrographic microscope because of the high concentration and the opacity of carbonaceous material in the matrix.

In situ Raman microprobe analyses of matrix graphite showed highly variable spectra (eight spectra collected, Fig. 6), often with a disordered D band greater than or comparable to the graphite G band. On the other hand, *in situ* Raman spectra of clast-hosted graphite (eight spectra collected, Fig. 7) were more consistent and illustrated a strong G band and a weak D band. *In situ* samples were rotated 360°, with Raman spectra collected at each 90° interval; only minor changes occured in the G- and D-band intensities, and slightly more so in S-band intensity (Fig. 9). Overall, all *in situ* Raman spectra had a relatively strong G band, which suggests a high degree of graphite crystallinity (Wopenka and Pasteris, 1993), though the differences between matrix graphite and clast-hosted graphite may be indicative of their different origins.

Some graphite particles are circular (Fig. 10C–U), and we term these particles graphite discs. Raman spectra of extracted graphite discs (Fig. 8) are highly consistent, comparable to those of clast-hosted graphite particles. Application of the graphite Raman geothermometer (Wopenka and Pasteris, 1993; Beyssac *et al.*, 2002; Rahl *et al.*, 2005) to these spectra suggests that these graphite discs experienced peak metamorphic temperatures of 513 ± 50°C (n = 12), which is broadly consistent with the amphibolite grade of the host rock, but slightly lower than the 600–650°C temperature estimate based on mineral association (Zhao *et al.*, 1999). Therefore, the carbonaceous precursors of these graphite discs were likely in place before or during the amphibolite metamorphism.

When observed via scanning electron microscopy, the extracted graphite particles are mostly irregularly shaped, with some discs (Fig. 10C–Q) and rare filaments (Fig. 10B). The filaments, *ca.* 1.5 μm in width and tens of μm in length, preserve no evidence for septation. The discs, which average about 60 μm in diameter (20–220 μm, s.d. = 31 μm, n = 270; Fig. 4) and 1–3 μm in thickness (Fig. 10N, 10S–T), are circular, ovate, and slightly elliptical in morphology, and they consist of graphite sheets (Fig. 10N–P). These discs and filaments are broadly similar in morphology to the acritarchs and filaments from the overlying Paleoproterozoic Hutuo Group in the same geographic region (Sun and Zhu, 1998). However, the Hutuo discs and filaments are poorly characterized; thus, at present, quantitative morphological comparisons cannot be ascertained.

Many specimens bear concentric (Fig. 10C–E) or crescentic (Fig. 10F–G, 10Q) marginal folds,

with isoclinal (Fig. 10F–G, 10L–M) or anticlinal (Fig. 10C–E) slopes. Some folds show plunging termination into the surface of the disc (arrow in Fig. 10D). Concentric and crescentic folds do not occur in the center of these discs, which are either flat (Fig. 10C, 10E–F, 10L, 10P–Q) or covered with irregularly arranged, fine wrinkles (Fig. 10H–J). The folds and wrinkles can be distinguished, on the basis of electron shadows in SEM observations using the secondary electron detector, from steps and kinks resulting from termination or dislocation of graphite sheets. At extremely high magnification, the graphite discs are characterized by nanoscale (10–100 nm) ridges and pores. The nanoridges bifurcate and anastomose (Fig. 10R), and their significance is obscure. The nanopores, when viewed with the backscatter detector, appear to be filled with an unidentified material that has an average atomic number greater than graphite (Fig. 10U). Similar nanopores (Fig. 10V), though an order of magnitude smaller in size, have been found in the vesicle walls of the Mesoproterozoic acritarch *Dictyosphaera delicata*, and are filled with aluminum phosphate minerals (Kaufman and Xiao, 2003).

Transmission electron microscopy showed that some discs appear to consist of two sets of graphite sheets, with a thin layer of electron-dense material between the sets (Fig. 10T). This is consistent with SEM observation of the naturally broken edge of a graphite disc (Fig. 10N), though in the latter specimen the two sets of graphite sheets are separated by a narrow gap.

Some morphological aspects of the graphite discs—and most of the irregular graphite particles—reflect graphite crystallization, overgrowth, inelastic deformation, and fragmentation. For example, the thickness of the discs may be variable due to graphite overgrowth (Fig. 10Q). The graphite discs may become somewhat subrounded, subhedral, or angular (Fig. 10H, 10L, 10P–Q), rather than curvilinear (Fig. 10C–G). The termination or dislocation of graphite sheets may form steps (arrow in Fig. 10P). A few specimens show very sharp bending (long arrow in Fig. 10O), kinking (short arrow in Fig. 10O), fracturing (long arrow in Fig. 10L), and fragmentation (arrows in Fig. 10H, 10K). Some discs consist of two distinct sets of graphite sheets, separated by a gap of <1 μm (Fig. 10N); this gap may result from physical separation along tabular cleavages. Features similar to these have been reported from metamorphic graphites from Grenville marbles and interpreted as overgrowths and deformation features (Kretz, 1996).

Five extracted graphite discs were analyzed for carbon isotopic signatures using a Cameca 6f ion microprobe. The results are intriguing but inconclusive (Table 2). In most cases, multiple analyzed spots on the same individual disc showed low variability of $\delta^{13}C$ values (2–3‰, three specimens), but the other specimens demonstrated greater intraspecimen variability (7–9‰, two specimens). Additionally, the range of values between different individuals spanned from -7.3 to -35.8‰ V-PDB. The mean $\delta^{13}C$ value of all ion probe measurements (-20.3‰ V-PDB) is similar to the -21.3‰ V-PDB value determined by standard techniques for bulk kerogen.

DISCUSSION

Graphite particles are common in Archean and younger metamorphic rocks, such as marbles, schists, and gneisses (Rakovan and Jaszczak, 2002; Ueno *et al.*, 2002; van Zuilen *et al.*, 2003; Satish-Kumar, 2005). Typically, metamorphic graphite is found in a few varying forms: well-developed crystals (Palache, 1941), deformed crystals (Kretz, 1996), crystals with microtopographic growth spirals (Rakovan and Jaszczak, 2002), crystals within graphite veins (along with many other minerals including quartz, sillimanite, ilmenite, and muscovite) (Rumble and Hoering, 1986), and in spheroidal or spherule aggregates (Jaszczak, 1997).

Based on isotopic studies and Raman analyses in conjunction with high-resolution transmission electron microscopy, it has been suggested that syngenetic graphite can form within metasedimentary rocks during metamorphic heating from the progressive crystallization of organic carbon within precursor sediments, whereby the original carbonaceous material becomes ordered into crystalline graphite (Weis *et al.*, 1981; Wopenka and Pasteris, 1993; Rantitsch *et al.*, 2004). Alternatively, some graphite forms are more likely to have formed by carbon precipitation from carbon-rich fluids (Rumble and Hoering, 1986; Satish-Kumar *et al.*, 2001; Jaszczak and Rakovan, 2002), by siderite decomposition (Fedo and Whitehouse, 2002; van Zuilen *et al.*, 2002, 2003), or by Fischer-Tropsch precipitation from CO_2–CH_4 fluids (Horita, 2005; McCollom and Seewald, 2006). Thus, the question arises whether the Jin-

gangku Formation graphite discs, characterized by such morphological features as marginal concentric folds, fine surficial wrinkles, and complex nanoridge and nanoporous structures, could have been morphologically shaped by metamorphic processes. If the circular morphology and concentric folds of these discs can be produced by metamorphism alone, then similar morphologies should be observed in other metamorphic graphite particles as well. However, to the best of our knowledge, no other graphite crystals have been shown to have similar morphological features that so distinctively characterize the Jingangku graphite discs (Palache, 1941; Kretz, 1996; Jaszczak, 1997; Rakovan and Jaszczak, 2002; Ueno *et al.*, 2002; van Zuilen *et al.*, 2003; Satish-Kumar, 2005). Instead, those graphite particles occur as interstitial crystals or inclusions in the common forms mentioned above, and their morphologies are probably unrelated to biology, though their ultimate carbon source may or may not be biological (Mojzsis *et al.*, 1996; Fedo and Whitehouse, 2002; van Zuilen *et al.*, 2003). Thus, it seems as though the morphology, micro-, and nano-scale structures of the Jingangku graphite discs cannot be accounted for by metamorphism alone.

The curvilinear margin of some Jingangku graphite discs is also difficult to account for by metamorphism alone. Abiotic precipitation of graphite is expected to produce hexagonal crystals. Such crystals may be deformed during metamorphism, but circular discs with concentric folds are not to be expected. If the Jingangku graphite discs were derived from amorphous kerogen, graphite overgrowth during metamorphism should reduce rather than enhance the marginal curvilinearity, and concentric folds are not to be expected, either. One may argue that gliding of graphite sheets in a directed stress environment could seemingly form crescentic marginal folds as illustrated in Fig. 10F–G, but the folds should have much sharper crests (Kretz, 1996; *e.g.*, Fig. 10O) and the disc center should show shearing in the same direction and magnitude as the margin. Additionally, bending or gliding of graphite sheets is not expected to generate regular concentric marginal folds.

Our inability to account for all morphologies of the Jingangku graphite discs by metamorphic processes alone compels us to consider other alternative interpretations. Is it possible that the Jingangku discs and filaments are graphitized biological structures? In this alternative interpretation, the filaments may represent filamentous bacteria, and the discs could represent originally spheroidal vesicles with a recalcitrant organic wall, which were subsequently deflated, flattened, and graphitized during compaction, diagenesis, and metamorphism. Their circular to ovate shape, marginal concentric folds, and surficial wrinkles are expected morphologies during the compression and elastic deformation of organic-walled vesicles; these features are commonly observed in compressed organic-walled microfossils in Proterozoic rocks (Schopf and Klein, 1992). Further, the nanoporous structures are similar to those found in Mesoproterozoic acritarchs, *i.e.*, *Dictyosphaera delicata* (Kaufman and Xiao, 2003). In addition, the gap between two sets of graphite sheets in some specimens (Fig. 10N), conservatively interpreted above as related to physical separation along tabular cleavages, may be alternatively interpreted as a gap between two compressed vesicle walls. Moreover, TEM observations show that some specimens have an electron-dense central layer (Fig. 10T), rather than a gap; this layer cannot be interpreted as cleavage separation but may represent material trapped within the compressed vesicle. Thus, we tentatively conclude that the graphite discs from the Jingangku Formation may represent deflated, flattened, and graphitized vesicles similar to acritarchs from younger rocks.

CONCLUSIONS

Key morphological features suggest biogenicity

Important features such as circular morphology, marginal folds, fine wrinkles, and trapped materials may have resulted from early diagenetic compression of spheroidal vesicles. Although these morphological features must have been altered during metamorphism and graphitization, hints of their presence may still be preservable in a fraction of the Jingangku graphite discs. Indeed, laboratory experiments demonstrate that Mesoproterozoic organic-walled microfossils (such as *Dictyosphaera delicata* and *Shuiyousphaeridium macroreticulatum*) heated within the hosting rock to 500°C over periods of up to 125 days show signs of graphitization, while retaining such features as discoidal morphology and concentric folds (Schiffbauer *et al.*, 2006).

Geochemical evidence inconclusive but consistent with biogenicity

A biological interpretation on the basis of morphological features described above implies that the ultimate carbon source of the Jingangku graphite discs must be biological as well. Carbonaceous material isolated from one of our samples has a bulk $\delta^{13}C$ value of −21.3‰ V-PDB, as determined by conventional combustion methods. Individual discs, measured using an ion microprobe (Kaufman and Xiao, 2003), show a wide range of $\delta^{13}C$ values from −7.4‰ to −35.9‰ V-PDB (mean = −20.3‰; n = 11; Table 2). Three of the individually analyzed graphite discs showed low variability (<3‰) of $\delta^{13}C$ values, but the other two specimens demonstrated much higher intraspecimen variability (7–9‰). These $\delta^{13}C$ values are inconclusive, given what is known about carbon isotope fractionations associated with abiotic processes. From experimental analyses, multiple abiotic pathways can lead to the synthesis of carbon compounds with $\delta^{13}C$ values as low as −60‰ due to kinetic isotope effects (Horita, 2005); moreover, it has been suggested that carbon compounds with $\delta^{13}C$ values as low as −30‰ (previously regarded as recycled sedimentary organic compounds) may be indigenous to the mantle (Horita, 2005). However, it is worth noting that the Jingangku specimens have a much wider $\delta^{13}C$ range and are more depleted in ^{13}C than graphite particles found in granulite-grade metamorphic rocks (Farquhar *et al.*, 1999; Santosh *et al.*, 2003; Satish-Kumar, 2005), where isotopic homogenization is presumably stronger. The range and heterogeneity of the Jingangku $\delta^{13}C$ values may record partial isotopic exchange during metamorphism (Ueno *et al.*, 2002), and the lowest measured values (*e.g.*, −35.9‰) are better approximations of primary $\delta^{13}C$ values. If so, then the measured $\delta^{13}C$ values may be stronger evidence for biological source than they appear.

Jingangku graphite particles have complex origins

It needs to be stressed that, though some irregular graphite particles in the Jingangku samples may be metamorphic or fragmentation products from circular graphite discs, it is unlikely that all of the graphite particles were derived from compressed vesicles. Indeed, carbonaceous extracts from unmetamorphosed fossiliferous rocks of younger age mainly consist of amorphous kerogen, and only a small fraction is represented by morphologically recognizable acritarchs. Nor is the carbon source of all Jingangku graphite particles biological. Petrographic evidence and Raman analyses discussed above suggest diverse origins of Jingangku graphite particles. It appears that the extracted graphite discs may have come from the clasts because of (1) the *in situ* observation that some graphite particles in clasts are circular (Fig. 3E–H), (2) the similarity between Raman spectra of clast-hosted graphite and extracted graphite discs (Figs. 7–8), and (3) the possibility that quartzite clasts may provide a shield against shearing deformation. However, this issue cannot be unambiguously resolved because of the limited resolution of *in situ* observation using light microscopy and the high concentration of matrix graphite. Thus, the Jingangku graphite particles may have complex origins, and we cannot conclusively disprove the possibility that both abiotic (*e.g.*, decomposition of ferrous carbonate minerals or Fischer–Tropsch precipitation from CO_2–CH_4 fluids catalyzed by Fe) and biotic processes may have contributed to the carbon source and morphology of the Jingangku graphite particles.

Highly metamorphosed rocks could retain highly altered but morphologically and geochemically recognizable signs of life

Despite the inconclusive nature of our interpretation, this study does suggest that, in our search for evidence of ancient life, more work should be directed to carbonaceous material even in highly metamorphosed rocks. Recent studies of Precambrian and Phanerozoic metamorphic rocks have recovered *bona fide* filamentous bacteria, organic-walled microfossils (*e.g.*, leiospheres, acanthomorphic acritarchs, and chitinozoans), and possible paraconodonts from greenschist-amphibolite-, and gneiss-grade metamorphic rocks (Kidder and Awramik, 1990; Knoll, 1992; Molyneux, 1998; Hanel *et al.*, 1999; Squire *et al.*, 2006; Zang, 2007). Thus, it is worthwhile to explore whether the taphonomic window for Archean life is wider than previously thought.

ACKNOWLEDGMENTS

This research was supported by the NASA Exobiology Program, National Science Foundation of China, Chinese Academy of Sciences, Chi-

nese Ministry of Science and Technology, State Key Laboratory of Paleobiology and Stratigraphy of the Chinese Academy of Sciences, Virginia Tech ASPIRES and ICTAS programs, the Virginia Space Grant Consortium, the Paleontological Society, and the Geological Society of America. We thank Y. Tian for field assistance; W. Huang (maceration), C. Wang (TEM), C. Farley (laser Raman microprobe), S. Mutchler (graphical assistance), E. Hauri and J. Wang (ion probe), and Y. Mao, J. Barry, and S.R.F. McCartney (SEM,Virginia Tech Institute for Critical Technologies and Applied Sciences) for technical help; and N. Butterfield, K. Grey, R. Law, R. Tracy, M. Kowalewski, and J.W. Huntley for discussion.

ABBREVIATIONS

FE-SEM, field emission scanning electron microscopy; IMF, instrumental mass fractionation; SEM, scanning electron microscopy; SHRIMP, Sensitive High Resolution Ion Microprobe; TEM, transmission electron microscopy; TOC, total organic carbon; V-PDB, Vienna Pee Dee Belemnite.

REFERENCES

Allwood, A.C., Walter, M.R., Kamber, B.S., Marshall, C.P., and Burch, I.W. (2006) Stromatolite reef from the Early Archean era of Australia. *Nature* 441, 714–718.

Altermann, W. and Schopf, J.W. (1995) Microfossils from the Neoarchean Campbell Group, Griqualand West Sequence of the Transvaal Supergroup, and their paleoenvironmental and evolutionary implications. *Precambrian Res.* 75, 65–90.

Awramik, S.M., Schopf, J.W., and Walter, M.R. (1983) Filamentous fossil bacteria from the Archean of Western Australia. *Precambrian Res.* 20, 357–374.

Bai, J. (1986) *The Early Precambrian Geology of Wutaishan*, Tianjin Science and Technology Press, Tianjin.

Bai, J., Wang, R.Z., and Guo, J.J. (1992) *The Major Geologic Events of Early Precambrian and Their Dating in Wutaishan Region*, Geological Publishing House, Beijing.

Bekker, A., Holland, H.D., Wang, P.-L., Rumble III, D., Stein, H.J., Hannah, J.L., Coetzee, L.L., and Beukes, N.J. (2004) Dating the rise of atmospheric oxygen. *Nature* 427, 117–120.

Beyssac, O., Goffé, B., Chopin, C., and Rouzaud, J.N. (2002) Raman spectra of carbonaceous material in metasediments: a new geothermometer. *Journal of Metamorphic Geology* 20, 859–871.

Brasier, M., McLoughlin, N., Green, O., and Wacey, D. (2006) A fresh look at the fossil evidence for early Archaean cellular life. *Philos. Trans. R. Soc. Lond., B, Biol. Sci.* 361, 887–902.

Brasier, M.D., Green, O.R., Jephcoat, A.P., Kleppe, A.K., Kranendonk, M.J.V., Lindsay, J.F., Steele, A., and Grassineau, N.V. (2002) Questioning the evidence for Earth's oldest fossils. *Nature* 416, 76–81.

Brasier, M.D., Green, O.R., Lindsay, J.F., McLoughlin, N., Steele, A., and Stoakes, C. (2005) Critical testing of Earth's oldest putative fossil assemblage from the 3.5 Ga Apex chert, Chinaman Creek, Western Australia. *Precambrian Res.* 140, 55–102.

Ding, T., Wan, D., Zhang, Z., Wang, C., and Li, Y. (2004) Sulfur isotope anomaly discovered in sulfide bed of later Archean Jingangku formation, Wutai group, Shanxi Province, China. *Geochim. Cosmochim. Acta* 68 (Supplement 1), A789.

Farquhar, J., Hauri, E., and Wang, J. (1999) New insights into carbon fluid chemistry and graphite precipitation: SIMS analysis of granulite facies graphite from Ponmudi, South India. *Earth Planet. Sci. Lett.* 171, 607–621.

Fedo, C.M. and Whitehouse, M.J. (2002) Metasomatic origin of quartz-pyroxene rock, Akilia, Greenland, and implications for Earth's earliest life. *Science* 296, 1449–1452.

Grotzinger, J.P. and Knoll, A.H. (1999) Stromatolites in Precambrian carbonates: evolutionary mileposts or environmental dipsticks? *Annu. Rev. Earth Planet. Sci.* 27, 313–358.

Grotzinger, J.P. and Rothman, D.H. (1996) An abiotic model for stromatolite morphogenesis. *Nature* 383, 423–425.

Hanel, M., Montenari, M., and Kalt, A. (1999) Determining sedimentation ages of high-grade metamorphic gneisses by their palynological record: a case study in the northern Schwarzwald (Variscan Belt, Germany). *International Journal of Earth Sciences* 88, 49–59.

Hofmann, H.J., Grey, K., Hickman, A.H., and Thorpe, R.I. (1999) Origin of 3.45 Ga coniform stromatolites in Warrawoona Group, Western Australia. *Geol. Soc. Am. Bull.* 111, 1256–1262.

Horita, J. (2005) Some perspectives on isotope biosignatures for early life. *Chem. Geol.* 218, 171–186.

Huntley, J.W., Xiao, S., and Kowalewski, M. (2006) 1.3 billion years of acritarch history: an empirical morphospace approach. *Precambrian Res.* 144, 52–68.

Jaszczak, J.A. (1997) Unusual graphite crystals from the Lime Crest quarry, Sparta, New Jersey. *Rocks and Minerals* 72, 330–334.

Jaszczak, J.A. and Rakovan, J. (2002) Growth spirals on graphite crystals from the Trotter Mine dump, Franklin, New Jersey. *The Picking Table* 43, 11–13.

Javaux, E.J., Knoll, A.H., and Walter, M.R. (2001) Morphological and ecological complexity in early eukaryotic ecosystems. *Nature* 412, 66–69.

Javaux, E.J., Knoll, A.H., and Walter, M.R. (2003) Recognizing and interpreting the fossils of early eukaryotes. *Orig. Life Evol. Biosph.* 33, 75–94.

Kaufman, A.J. and Xiao, S. (2003) High CO_2 levels in the Proterozoic atmosphere estimated from analyses of individual microfossils. *Nature* 425, 279–282.

Kidder, D.L. and Awramik, S.M. (1990) Acritarchs in lower greenschist facies argillite of the middle Proterozoic Libby Formation, Upper Belt Supergroup, Montana. *Palaios* 5, 124–133.

Knoll, A.H. (1992) Microfossils in metasedimentary cherts of the Scotia Group, Prins Karls Forland, western Svalbard. *Palaeontology* 35, 751–774.

Knoll, A.H. (1994) Proterozoic and Early Cambrian protists: Evidence for accelerating evolutionary tempo. *Proc. Natl. Acad. Sci. U.S.A.* 91, 6743–6750.

Knoll, A.H. and Barghoorn, E.S. (1977) Archean microfossils showing cell-division from Swaziland System of South Africa. *Science* 198, 396–398.

Knoll, A.H., Javaux, E.J., Hewitt, D., and Cohen, P. (2006) Eukaryotic organisms in Proterozoic oceans. *Philos. Trans. R. Soc. Lond., B, Biol. Sci.* 361, 1023–1038.

Kretz, R. (1996) Graphite deformation in marble and mylonitic marble, Grenville Province, Canadian Shield. *Journal of Metamorphic Geology* 14, 399–412.

Kröner, A., Wilde, S.A., Li, J.H., and Wang, K.Y. (2005) Age and evolution of a late Archean to Paleoproterozoic upper to lower crustal section in the Wutaishan/Hengshan/Fuping terrain of northern China. *Journal of Asian Earth Sciences* 24, 577–595.

Lepland, A., van Zuilen, M.A., Arrhenius, G., Whitehouse, M.J., and Fedo, C.J. (2005) Questioning the evidence for Earth's earliest life—Akilia revisited. *Geology* 33(1), 77–79.

Li, J.L., Wang, K.Y., Wang, C.Q., Liu, X.H., and Zhao, Z.Y. (1990) Early Proterozoic collision orogenic belt in Wutaishan area, China. *Scientia Geologica Sinica* 25, 1–11.

Liu, D.Y., Page, R.W., Compston, W., and Wu, J.S. (1985) U-Pb zircon geochronology of late Archean metamorphic rocks in the Taihangshan-Wutaishan area, North China. *Precambrian Res.* 27, 85–109.

Lowe, D.R. (1994) Abiotic origin of described stromatolites older than 3.2 Ga. *Geology* 22, 387–390.

McCollom, T.M. and Seewald, J.S. (2006) Carbon isotope composition of organic compounds produced by abiotic synthesis under hydrothermal conditions. *Earth Planet. Sci. Lett.* 243, 74–84.

Mojzsis, S.J. and Harrison, T.M. (2000) Vestiges of a beginning: clues to the emergent biosphere recorded in the oldest known sedimentary rocks. *GSA Today* 10, 1–6.

Mojzsis, S.J., Arrhenius, G., McKeegan, K.D., Harrison, T.M., Nutman, A.P., and Friend, C.R.L. (1996) Evidence for life on Earth by 3800 million years ago. *Nature* 384, 55–59.

Molyneux, S.G. (1998) An upper Dalradian microfossil reassessed. *J. Geol. Soc. London* 155, 741–743.

Palache, C. (1941) Contributions to the mineralogy of Sterling Hill, New Jersey: Morphology of graphite, arsenopyrite, pyrite, and arsenic. *Am. Mineral.* 26, 709–717.

Polat, A., Kusky, T., Li, J., Fryer, B., Kerrich, R., and Patrick, K. (2005) Geochemistry of Neoarchean (*ca.* 2.55–2.50 Ga) volcanic and ophiolitic rocks in the Wutaishan greenstone belt, central orogenic belt, North China craton: Implications for geodynamic setting and continental growth. *GSA Bulletin* 117, 1387–1399.

Rahl, J.M., Anderson, K.M., Brandon, M.T., and Fassoulas, C. (2005) Raman spectroscopic carbonaceous material thermometry of low-grade metamorphic rocks: calibration and application to tectonic exhumation in Crete, Greece. *Earth Planet. Sci. Lett.* 240, 339–354.

Rakovan, J. and Jaszczak, J.A. (2002) Multiple length scale growth spirals on metamorphic graphite {001} surfaces studied by atomic force microscopy. *Am. Mineral.* 87, 17–24.

Rantitsch, G., Grogger, W., Teichert, C., Ebner, F., Hofer, C., Maurer, E., Schaffer, B., and Toth, M. (2004) Conversion of carbonaceous material to graphite within the Greywacke Zone of the Eastern Alps. *International Journal of Earth Sciences* 93, 959–973.

Rosing, M.T. (1999) ^{13}C-depleted carbon microparticles in >3700-Ma sea-floor sedimentary rocks from West Greenland. *Science* 283, 674–676.

Rumble, D. and Hoering, T.C. (1986) Carbon isotope geochemistry of graphite vein deposits from New Hampshire, U.S.A. *Geochim. Cosmochim. Acta* 50, 1239–1247.

Santosh, M., Wada, H., Satish-Kumar, M., and Binu-Lal, S.S. (2003) Carbon isotope "stratigraphy" in a single graphite crystal: implications for the crystal growth mechanism of fluid-deposited graphite. *Am. Mineral.* 88, 1689–1696.

Satish-Kumar, M. (2005) Graphite-bearing CO_2-fluid inclusions in granulites: insights on graphite precipitation and carbon isotope evolution. *Geochim. Cosmochim. Acta* 69, 3841–3856.

Satish-Kumar, M., Wada, H., Santosh, M., and Yoshida, M. (2001) Fluid-rock history of granulite facies humite-marbles from Ambasamudram, southern India. *Journal of Metamorphic Geology* 19, 395–410.

Schiffbauer, J.D., Xiao, S., Bodnar, R.J., Yin, L., Yuan, X., Meng, F., Hu, J., and Kaufman, A.J. (2006) Can organic-walled microfossils survive high metamorphic heating? Characterization of experimentally heated acritarchs using Raman spectroscopy. [abstract]. *GSA Abstracts and Programs* 38(7), 305.

Schopf, J.W. (1993) Microfossils of the Early Archean Apex chert: new evidence of the antiquity of life. *Science* 260, 640–646.

Schopf, J.W. and Klein, C. (1992) *The Proterozoic Biosphere: A Multidisciplinary Study,* Cambridge University Press, Cambridge.

Schopf, J.W., Kudryavtsev, A.B., Agresti, D.G., Wdowiak, T.J., and Czaja, A.D. (2002) Laser-Raman imagery of Earth's earliest fossils. *Nature* 416, 73–76.

Schopf, J.W. and Packer, B.M. (1987) Ealry Archean (3.3-billion- to 3.5-billion-year-old) microfossils from Warrawoona group, Australia. *Science* 237, 70–73.

Schopf, J.W. and Walter, M.R. (1983) Archean microfossils: new evidence of ancient microbes. In *Earth's Earliest Biosphere: Its Origin and Evolution*, edited by J.W. Schopf, Princeton University Press, Princeton, NJ, pp. 214–239.

Squire, R.J., Stewart, I.R., and Zang, W.L. (2006) Acritarchs in polydeformed and highly altered Cambrian rocks in western Victoria. *Australian Journal of Earth Sciences* 53, 697–705.

Sun, S. and Zhu, S. (1998) The discovery of micropaleophytes from the Doucun Subgroup, Hutuo Group in Wutai Mountain, Shanxi, China. *Acta Micropalaeontologica Sinica* 15, 286–293.

Tian, Y.Q. (1991) *Geology and Gold Mineralization of Wutai–Hengshan Greenstone Belt*. Shanxi Science and Technology Press, Taiyuan.

Ueno, Y., Yurimoto, H., Yoshioka, H., Komiya, T., and Maruyama, S. (2002) Ion microprobe analysis of graphite from *ca.* 3.8 Ga metasediments, Isua supracrustal belt, West Greenland: Relationship between metamorphism and carbon isotopic composition. *Geochim. Cosmochim. Acta* 66, 1257–1268.

van Zuilen, M.A., Lepland, A., and Arrhenius, G. (2002) Reassessing the evidence for the earliest traces of life. *Nature* 418, 627–630.

van Zuilen, M.A., Lepland, A., Teranes, J., Finarelli, J., Wahlen, M., and Arrhenius, G. (2003) Graphite and carbonates in the 3.8-Ga-old Isua Supracrustal Belt, southern West Greenland. *Precambrian Res.* 126, 331–348.

Vidal, G. and Moczydlowska-Vidal, M. (1997) Biodiversity, speciation, and extinction trends of Proterozoic and Cambrian phytoplankton. *Paleobiology* 23, 230–246.

Walsh, M.M. and Lowe, D.R. (1985) Filamentous microfossils from the 3,500-myr-old Onverwacht Group, Barberton Mountain Land, South Africa. *Nature* 314, 530–532.

Wang, K.Y., Li, J.L., Hao, J., Li, J.H., and Zhou, S.P. (1996) The Wutaishan orogenic belt within the Shanxi Province, northern China: a record of late Archaean collision tectonics. *Precambrian Res.* 78, 95–103.

Wang, K.Y., Hao, J., Wilde, S., and Cawood, P. (2000) Reconsideration of some key geological problems of late Archean–early Proterozoic in the Wutaishan-Hengshan area: constraints from SHRIMP U–Pb zircon data. *Scientia Geologica Sinica* 35, 175–184.

Weis, P.L., Friedman, I., and Gleason, J.P. (1981) The origin of epigenetic graphite: evidence from isotopes. *Geochim. Cosmochim. Acta* 45, 2325–2332.

Wilde, S.A., Cawood, P., Wang, K.Y., and Nemchin, A. (1997) The relationship and timing of granitoid evolution with respect to felsic volcanism in the Wutai Complex, North China Craton. *Proceedings of the 30th International Geological Conference: Precambrian Geology and Metamorphic Petrology* 17, 75–88.

Wilde, S.A., Cawood, P.A., Wang, K.Y., Nemchin, A., and Zhao, G.C. (2004a) Determining Precambrian crustal evolution in China: a case-study from Wutaishan, Shanxi Province, demonstrating the application of precise SHRIMP U–Pb geochronology. In *Aspects of the Tectonic Evolution of China, Special Publication 226*, edited by J. Malpas, C.J.N. Fletcher, J.R. Ali, and J.C. Aitchison, Geological Society of London, London, pp. 5–25.

Wilde, S.A., Zhao, G.C., Wang, K.Y., and Sun, M. (2004b) First SHRIMP zircon U–Pb ages for Hutuo Group in Wutaishan: Further evidence for palaeoproterozoic amalgamation of North China Craton. *Chin. Sci. Bull.* 49, 83–90.

Wilde, S.A., Cawood, P.A., Wang, K.Y., and Nemchin, A.A. (2005) Granitoid evolution in the Late Archaean Wutai Complex, North China Craton. *Journal of Asian Earth Sciences* 24, 597–613.

Wopenka, B. and Pasteris, J.D. (1993) Structural characterization of kerogens to granulite-facies graphite: applicability of Raman microprobe spectroscopy. *Am. Mineral.* 78, 533–557.

Xiao, S., Knoll, A.H., Kaufman, A.J., Yin, L., and Zhang, Y. (1997) Neoproterozoic fossils in Mesoproterozoic rocks? Chemostratigraphic resolution of a biostratigraphic conundrum from the North China Platform. *Precambrian Res.* 84, 197–220.

Yuan, G.P. and Zhang, R.Y. (1993) The structural environment of the paleorift in Wutai greenstone belt. *Shanxi Geology* 8, 21–28.

Zang, W.-L. (2007) Deposition and deformation of late Archaean sediments and preservation of microfossils in the Harris Greenstone Domain, Gawler Craton, South Australia. *Precambrian Res.* 156, 107–124.

Zhao, G., Cawood, P., and Lu, L. (1999) Petrology and P–T history of theWutai amphibolites: implications for tectonic evolution of the Wutai Complex, China. *Precambrian Res.* 93, 181–199.

Zhao, G., Sun, M., Wilde, S.A., and Guo, J. (2004) Late Archean to Paleoproterozoic evolution of the Trans-North China Orogen: insights from synthesis of existing data from the Hengshan-Wutai-Fuping belt. In *Aspects of the Tectonic Evolution of China, Special Publication 226*. edited by J. Malpas, C.J.N. Fletcher, J.R. Ali, and J.C. Aitchison, Geological Society of London, London, pp. 27–55.

Address reprint requests to:
James D. Schiffbauer
4044 Derring Hall
Department of Geosciences
Virginia Polytechnic Institute and State University
Blacksburg VA 24061

E-mail: jdschiff@vt.edu